Validation of a two-step simplified compatible homogenisation approach extended to out-plane loaded masonries

Elisa Bertolesi

ICITECH,
Universitat Politècnica de Valencia,
Camino de Vera s/n 46022,
Valencia, Spain
Email: elber4@upv.es

Luis Carlos Silva

Department of Civil Engineering,
ISISE,
University of Minho,
Azurém, 4800-058 Guimarães, Portugal
Email: luisilva.civil@gmail.com

Gabriele Milani*

Department of Architecture,
Built Environment and Construction engineering (ABC),
Politecnico di Milano,
Piazza Leonardo da Vinci 32,
20133, Milan, Italy
Email: gabriele.milani@polimi.it
*Corresponding author

Abstract: A two-step homogenisation model, formulated by the authors for the in-plane case, is herein extended for the nonlinear out-of-plane analysis of masonry structures. A rectangular running bond elementary cell is discretised by 24 elastic CST elements and inelastic zero-thickness interfaces. The mechanical meso-scale problem is briefly recalled, whereas the out-of-plane homogenised behaviour is evaluated by means of a simple on-thickness integration of the in-plane homogenised curves. At a macro-scale, the rigid body and spring model is slightly modified to allow both flexural and torsional failure mechanisms. The validation of the numerical approach is achieved comparing with some full-scale masonry panels tested in two-way bending up to failure. A series of nonlinear structural analyses are conducted considering different parameters, which have been varied during the experimental campaign. The numerical results are promising and demonstrate the capability to deal with different failure mechanisms as result of a combination of various experimental aspects.

Keywords: masonry; in-plane loads; out of plane loads; semi-analytical approach; compatible model of homogenisation.

Reference to this paper should be made as follows: Bertolesi, E., Silva, L.C. and Milani, G. (2019) 'Validation of a two-step simplified compatible homogenisation approach extended to out-plane loaded masonries', *Int. J. Masonry Research and Innovation*, Vol. 4, No. 3, pp.265–296.

Biographical notes: Elisa Bertolesi holds a PhD in Architecture, Built Environment and Construction Engineering (obtained in 2017) at the Technical University of Milan, Italy and MSc (2012) in 'Ingegneria dei Sistemi Edilizi' at the same university. She is currently a Post-doc Research Fellow at the Technical University of Valencia, Spain. She is an expert in masonry numerical analysis by means of combined homogenisation and rigid body and spring model techniques (HRBSM), both in the nonlinear static and dynamic fields. Her research interest covers also strengthening with FRP, FRCM and TRM. In 2016, she won the International Masonry Society Postgraduate Student Award by the International Masonry Society IMS.

Luis Carlos Silva holds an MSc (2013) in Civil Engineering from the University of Minho. After working one year as a structural engineer, he is currently a PhD candidate at ISISE, in the same university and within a FCT scholarship, under the supervision of Professor Paulo B. Lourenço and Professor Gabriele Milani. His research interests are the structural analysis of masonry structures with focus on cultural heritage constructions; the in- and out-of-plane dynamic analysis of masonry structures; homogenisation procedures and finite element modelling and risk analysis.

Gabriele Milani is an Associate Professor of Structural Mechanics at the Politecnico di Milano, Italy. So far, he has authored more than 160 papers on international journals and edited a book. He is the second author in Scopus under the keyword 'masonry'. He has been awarded an ICE Telford Premium, a most cited author by *Computers & Structures* and a Bathe award. He is the Editor-in-Chief of two international journals.

1 Introduction

Masonries have been used for centuries to build a variety of different constructions. As clearly visible in the damages surveyed after earthquakes, seismic resistant criteria have not been considered a prerequisite for the design of load bearing members of a wide portion of the built heritage (Brandonisio et al., 2013; Augenti and Parisi, 2010; Çelebi et al., 2010; Parisi and Augenti, 2013). As a matter of fact, lateral loads, such as those induced by seismic events have been ignored in favour of a simplified design-based only on gravity loads. Unfortunately, the high seismic hazard of some European countries (as Italy for instance) in addition to the low or negligible tensile strength and high weight of the masonry material, had adversely influenced the behaviour of such constructions against out of plane loads, and sometimes they had led them to collapse (Augenti and Parisi, 2010; Çelebi et al., 2010; Parisi and Augenti, 2013; de Felice and Giannini, 2001; Shawa et al., 2012). Ancient constructions often shown to fail due to the progressive separation of the whole building into single elements that behave independently one from the other. In such a situation, the collapse of the single masonry membranes may anticipate the global collapse of the structure. In this framework, the presence of an adequate interlocking between perpendicular walls may assume a relevant importance

when dealing with such type of constructions. As a matter of fact, lateral play a crucial, being the out of plane rocking of facades one of the most frequent failure mechanisms exhibited by ancient by ancient masonries (Craig et al., 2004; Griffith and Magenes, 2003; Wilhelm et al., 2007; Dazio, 2008). Even among more recent constructions, the presence of good lateral restraints can significantly modify the failure pattern exhibited by such structures. Indeed, masonry walls can be can be subjected to one or two ways bending depending on the lateral connections.

From both experimental experience and post-earthquake surveys, it appears clear that out of plane damages are very common for slender walls, for which it is acceptable to assume that masonry behaves as a thin Kirchhoff-Love plate (Craig et al., 2004; Griffith and Magenes, 2003; Dazio, 2008), so that, at the macro-scale, almost every out of plane damage mechanism can be heuristically described as a combination of three fundamental mechanisms, namely vertical bending, horizontal bending and torsion.

Another important issue is the role played by the static vertical compression, mainly due to gravity loads. It is well known, indeed, that vertical pre-compression changes considerably the moment-curvature nonlinear relationships at a sectional level, and, in conjunction with bricks staggering (i.e., the actual masonry texture), has an effect on both vertical and horizontal bending.

Orthotropy is another feature related to texture. Especially for the case of 'vertical' bending (we define vertical a bending with rotation vector parallel to the vertical axis), bed joints tend to contribute on the increase of the load carrying capacity. Mainly, the different topology of the continuous horizontal mortar joints when compared to the vertical ones, interrupted by the blocks, implies that the tangential stresses arising on mortar bed joints tend to play a significant role in the vertical bending increase, while they substantially vanish in the horizontal bending response. In addition, it has been shown that the masonry texture produces perceivable effects that tend to become more and more evident with the progressive degradation of the material.

In the past 30 years, research focused mostly on experimentation, with the aim of suggesting to the designer at least phenomenological rules. Nevertheless, also experimental studies have been very limited and concerned solely with measurements of the flexural strength mostly for the case when the plane of failure occurs parallel to the bed joints, while elastic and inelastic properties have usually been ignored.

Two ways have been followed until now:

a To study the overall behaviour of full scale masonry structures by means of experimental investigations. Such laboratory tests are frequently costly due to the fact that ad hoc set-ups have to be prepared.

b To test the behaviour of in scale masonry prototypes. Even in this case, the experimental investigation may become costly.

A third option is represented by the possibility to analyse single unreinforced masonry elements. In this case, various aspects can be considered during the tests even if in a simplified manner. Furthermore, another aspect that should be investigated better from an experimental viewpoint is of course the influence of membrane forces (always present in actual structures as heavy dead vertical loads). It is evident, in fact, that these actions strongly influence the out of plane failure resistance of the brickwork, especially for what concerns the horizontal bending. A combined membrane/flexural experimentation has been conducted in the past only by few authors. Among these, the contributions by

Mojsilovic and Marti (1994) on reinforced pre-stressed wall specimens and by Guggisberg and Thürlimann (1990) on masonry walls subjected to vertical normal load and combined bending/twisting moments are worth noting.

The prediction of the behaviour beyond elasticity (and in particular of the ultimate load bearing capacity) of masonry walls out of plane loaded is paramount for both the design of new structures and the safety assessment of existing masonry buildings. Out of plane failures are very common in presence of deformable floors and occur always at very low levels of horizontal actions, especially for historical buildings with poor mechanical properties of the joints and for slender perimeter walls (Brandonisio et al., 2013; Augenti and Parisi, 2010; Çelebi et al., 2010; Parisi and Augenti, 2013).

Only in recent years, some numerical tools based on linear and nonlinear FE and DE methods specifically developed for out of plane actions have been presented and tested on actual engineering cases, see, e.g., (Milani et al., 2006; Casolo, 1999; Orduña, 2003; Johnson, 1996; Milani et al., 2005; Cecchi et al., 2005; Reccia et al., 2014; Lemos, 2007; Sincraian, 2001; Baraldi and Cecchi, 2017).

Basically, three different approaches have been proposed for the design at ultimate limit state. They can be classified as:

1 empirical methods based on experimental evidences

2 incremental procedures based on nonlinear FE codes (within continuum and/or a discrete approach)

3 yield or fracture line methods based on limit analysis.

Apart from experimentation, it is worth noting that a FE nonlinear analysis is probably the most indicated for a reliable investigation of the problem.

Nevertheless, it is not yet clear how it is possible to characterise completely (from a mechanical viewpoint) an ‘equivalent macro-model’ to introduce as input in a FE code. In the same way, a ‘micro-mechanical approach’ seems to be hardly applicable for practical purposes, since too many elements are required for the nonlinear analysis even for small masonry specimens. The third possibility is represented by homogenisation techniques; nevertheless, the advantage of substituting the micro-structure with averaged macroscopic quantities can be considered effective only if a FE discretisation at a cell level is avoided.

On the other hand, an approach based on limit analysis seems to be prompt to apply in practice. For this reason, it was utilised successfully in the past by several authors, such as for instance by Sinha (1978, 1980), de Felice and Giannini (2001), Reccia et al. (2014) and Borri (2004), who applied the method as a first evaluation of the damages induced by the Umbria-Marche earthquake, 1997. Furthermore, and as already pointed out, this method has been introduced in the British Masonry standard, probably for its simplicity in practical design combined with the reliability of the results obtained in terms of failure load. Nevertheless, its applicability to masonry structures is not immediate, since a full mechanical characterisation at a macro-scale is required if we want to estimate the internal power dissipated along generic fracture lines and apply the limit analysis theorems. For these reasons, homogenisation theory combined with limit analysis seems to be a very powerful tool for obtaining the failure polytopes of the homogenised material, so making possible a structural analysis at collapse via the classical yield-line theory or FE limit analyses (Milani et al., 2006; Casolo, 1999;

Orduña, 2003; Johnson, 1996; Milani et al., 2005; Cecchi et al., 2005; Capurso, 1971; Sab, 2003; de Buhan and de Felice, 1997; Sutcliffe et al., 2001).

In the present paper, a simplified two-step nonlinear homogenisation model, previously formulated by the authors to deal with in-plane loaded masonries, is extended to out of plane loads by simple on thickness integration of the in-plane model. Whilst the procedure is certainly a simplified one, it proved to be reasonably accurate for sufficiently thin walls (i.e., under Kirchhoff-Love hypotheses), and hence suitable for running bond masonry.

For validation purposes, some laboratory tests performed by Griffith and Vaculik (2007) on a series of unreinforced masonries in two-way bending have been considered. The experimental campaign comprises three groups of panels, called type A, type B and type C and differing one each other either for the geometry or the level of vertical in plane pre-compression, as it will be discussed in detail in the sequel.

The paper is organised into three parts. The first sections are devoted to the introduction of the in-plane model, which is briefly discussed. In this context, the extension of the in-plane homogenisation model to out of plane actions is presented. The derivation of the moment-curvature relationships used to describe numerically the out of plane nonlinear behaviour is shown with applicative examples.

The second part is aimed at reviewing the experimental campaign performed by Griffith and Vaculik (2007). The pressure-displacement curves as well as the damage patterns obtained at failure are recalled for all the examples considered. In the last part of the paper, the homogenisation model is benchmarked on such panels. Some sections are devoted to the discussion of the results obtained at cell level, with emphasis on the moment-curvature relationships deduced using the extended version of the proposed procedure. Finally, the numerical results obtained at structural level are comparatively assessed with respect to:

1 deformed shapes at collapse of the panels

2 global behaviours (i.e., pressure-displacement diagrams)

3 damage patterns obtained, separately for horizontal, vertical bending and torsion.

2 In-plane two step simplified compatible homogenised approach

The proposed in-plane two-step homogenisation approach is herein briefly recalled, for a detailed description of the proposed model the reader is referred to Bertolesi et al. (2016) and Milani and Bertolesi (2017). The first step of the two-step procedure is applied at the meso-scale, where the assemblage of bricks and mortar constituting the unreinforced elementary cell is substituted with a macroscopic equivalent material through a so called compatible identification, a peculiar homogenisation technique already adopted by the authors in a variety of different contexts (see for instance, Bertolesi et al., 2016; Milani and Bertolesi, 2017). The unit cell is discretised with 24 elastic constant stress triangles used to model the bricks, whereas mortar joints are reduced to zero-thickness inelastic interfaces. Holonomic constitutive relationships between micro-stresses (normal σ and tangential τ) and total jumps of displacements adopted are multi-linear and the homogenisation problem path independent. A coupling between normal and shear stresses, typically ruled by a frictional-cohesive law (Mohr-Coulomb criterion) is

imposed on interfaces. The tensile and tangential strengths of the mortar material (f_n^I and f_t^{II}) are calibrated in agreement with experimental data provided by Griffith and Vaculik (2007), as described in the following sections.

The in-plane nonlinear homogenised stress-strain relationships are obtained stretching the elementary cell horizontally and vertically for the determination of Σ_{xx} and Σ_{yy} respectively, and assuming a homogeneous shear deformation state incremented up to failure to evaluate Σ_{xy}.

The second step is performed at a structural level and relies into the implementation of the homogenised stress-strain relationships previously determined into a rigid element approach (also known as RBSM), where masonry continuum is discretised by quadrilateral rigid elements interconnected by shear and normal equivalent inelastic homogenised springs.

Such procedure, already utilised in the past to tackle similar problems in the nonlinear static and dynamic case, has the advantage that meso- and macro-scale are fully decoupled, i.e., homogenised stress-strain nonlinear relationships of the springs connecting rigid elements are evaluated in step 1, without the need of solving new boundary value problems at each load step in each Gauss point.

Figure 1 Micro-mechanical model proposed (a) geometric properties of the elementary cell (b) anti-periodicity of the micro-stress field (c) periodic displacement field (see online version for colours)

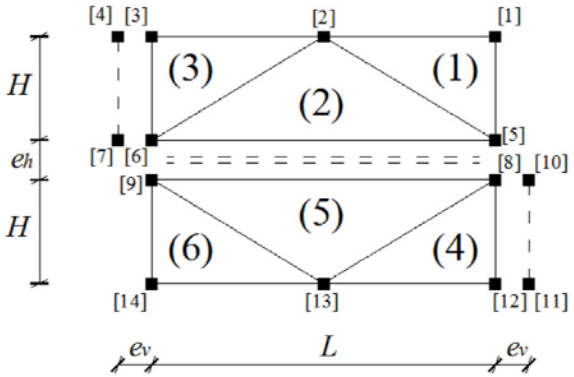

(a)

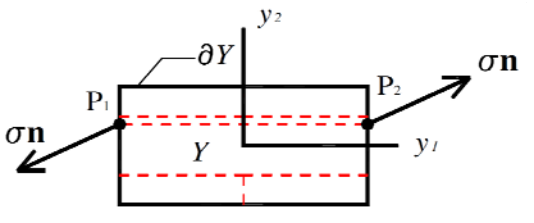

(b)

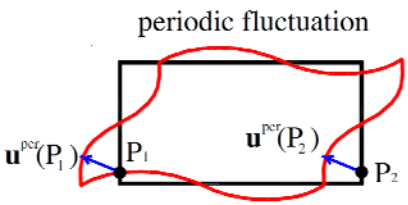

(c)

3 Extension to the out of plane failure mechanisms

In the present section, the homogenisation model herein presented is extended to the out of plane failure mechanisms. The discrete model is conceived to allow the description of three different out of plane failures: horizontal and vertical bending as well as torsion (see Figure 2).

Figure 2 Failure mechanisms allowed in the proposed homogenisation model (a) horizontal bending (b) vertical bending (c) torsion (see online version for colours)

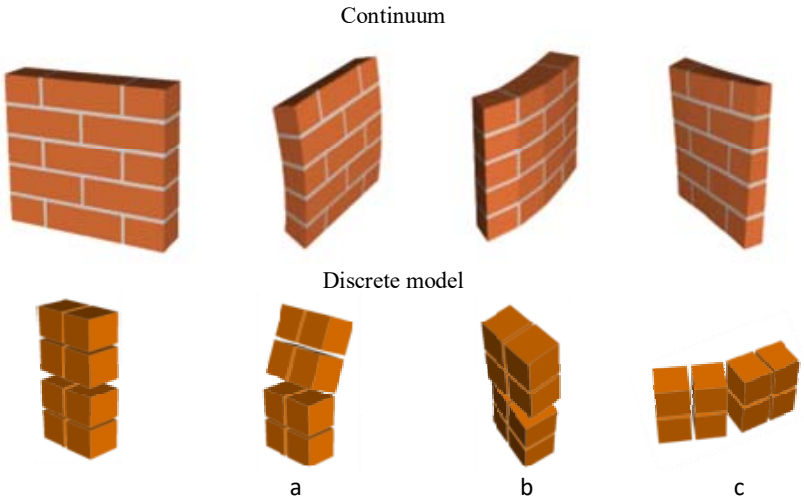

The extension herein presented is performed starting from the discrete model used to study the in plane loaded masonries, so that infinitely resistant quadrilateral elements are assumed with deformable interfaces placed along two different angles: 0 and 90 degrees. The behaviour of the interfaces is orthotropic with softening, because it derives from the homogenisation strategy previously recalled.

Figure 3 Geometry of the discrete model in case of horizontal bending (see online version for colours)

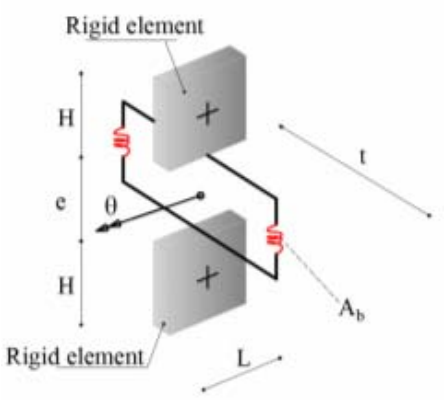

Similarly to the in plane case, the identification of the mechanical properties to be used in the discrete model is performed adopting an energetic equivalence.

Let us suppose to apply a horizontal (or vertical) bending to the discrete model as depicted in Figure 3.

The energies stored by the continuum (Π_e) and discrete (Π_d) models are the following:

$$\prod_e = \frac{1}{2} D_{yy} \chi^2 \frac{(H+e)L}{2} \tag{1}$$

$$\prod_d = \frac{1}{2} K_\vartheta \vartheta^2 \tag{2}$$

where $D_{yy} = \frac{E_{yy} t^3}{12\left(1-v_{xy}^2\right)}$ and $K_\vartheta \theta = 2\frac{t}{2} E_t A_b \frac{t}{2}\frac{2}{e}\vartheta = E_t A_b \frac{t^2}{e}\vartheta$.

Equating the two energies and assuming $\vartheta = \chi(H+e)$, the homogenised elastic modulus in case of horizontal bending E_t is obtained as follows:

$$E_t = E_{yy} \frac{te}{12\left(1-v_{xy}^2\right)} \frac{L}{2(H+e)A_b} \tag{3}$$

It is worth noting that 't' is the thickness of the considered masonry, L and H are the geometries of the rigid elements of the discrete model, 'e' is the distance between two contiguous rigid quadrilateral elements and A_b is the area of each truss elements. An analogous procedure can be adopted for vertical bending.

If we suppose to apply a torsion to the model, the following energies are derived:

$$\prod_e = \frac{1}{2} 2 D_t \chi_t^2 (H+e)(L+e) \tag{4}$$

$$\prod_d = \frac{1}{2}\left(K_X^t \left(2\vartheta_Y^t\right)^2 + K_Y^t \left(2\vartheta_X^t\right)^2\right) \tag{5}$$

And hence:

$$\prod_d = \frac{eL^3}{2t} E_s^t \vartheta_Y^{t^2} + \frac{eH^3}{2t} E_s^t \vartheta_X^{t^2} \tag{6}$$

Assuming: $D_t = \frac{Gt^3}{12}$, $\vartheta_X^t = \chi_t \frac{(H+e)}{2}$ and $\vartheta_Y^t = \chi_t \frac{(L+e)}{2}$ we get the following expression:

$$\frac{3}{2}\frac{e}{t^4} \frac{\left(L^3(L+e)^2 + H^3(H+e)^2\right)}{(H+e)(L+e)} E_s^t = G \tag{7}$$

Expression (7) allows determining E_s^t that is the elastic modulus of the homogenised torque spring elements. The other geometrical parameters have been defined in the previous case, whereas G is the shear modulus of masonry.

Such expression can be further simplified when $L = H$. In this case, equation (7) is modified into equation (8), i.e., as follows:

$$E_s^t = \frac{1}{3} G \frac{t^4}{eH^3} \tag{8}$$

The procedure described in what follows is required to convert the latter information in valid input data for the FE package used at a macro scale. To accomplish this, obtaining stress and strain curves for each angle of the interface and for each bending moment direction is mandatory. Thus, the material orthotropy can be reproduced by defining different input stress-strain relationships according to the trusses plane. The conversion between bending and torsion moments and stress-strain values has been achieved by the following equations:

$$\sigma_{horizontal\ bending} = \frac{M_{xx} H}{2 A_{by} t} \quad \varepsilon_{horizontal\ bending} = \frac{\vartheta t}{e} \tag{9}$$

$$\sigma_{vertical\ bending} = \frac{M_{yy} L}{2 A_{bx} t} \quad \varepsilon_{vertical\ bending} = \frac{\vartheta t}{e} \tag{10}$$

$$\sigma_{torsion} = \frac{ML}{A_{bxy} L} \quad \varepsilon_{torsion} = \frac{\vartheta L/2}{t} \tag{11}$$

Here, M is the bending moment, A_{bx} (A_{by}) is the area of the truss elements placed along x direction (y direction) and A_{bxy} is the torque truss area, e is the gap between the rigid plates, which ideally should be zero but in practice is assumed small enough to be able to place trusses between elements and t is the thickness of the considered masonry wall.

4 Experimental data used: benchmark panels

A series of eight full scale walls were tested by Griffith and Vaculik (2007) to investigate the out of plane behaviour of existing unreinforced masonry panels. This information is briefly described here and used to validate the present numerical procedure. A single leaf running bond pattern was obtained using ten-hole cored clay brick units with dimensions $230 \times 76 \times 110$ mm^3 and 10 mm thick mortar joints. All the panels were loaded through airbags placed on the outer surface in order to subject the return walls to compression. Several parameters were varied during the experimental campaign, such as the overall geometry of the walls, the presence of openings, the restraint conditions and finally, the level of the vertical pre-compression load. In Figure 4 all the typologies of the as built panels are depicted: with the label type A authors refer to the solid walls, windowed samples are indicated as type B, whereas type C is used for the square walls. An indication of the level of pre-compression used for each sample is even present in Figure 4. Panels belonging to type B differ from type A for the presence of an eccentric opening with dimensions equal to $1{,}000 \times 1{,}200$ mm^2 located at 650 mm from the left hand side of the wall. A central window with dimensions of $1{,}000 \times 1{,}200$ mm^2 located symmetrically with respect to the two ends is provided for panels W7 and W8 (i.e., type C). In the next section, each group of walls is briefly re-analysed from an experimental point of view, showing the global pressure vs. displacements curves

obtained during the laboratory tests and the crack patterns provided at failure by Griffith and Vaculik (2007).

Figure 4 Typologies of masonry panels tested by Griffith and Vaculik (2007) (see online version for colours)

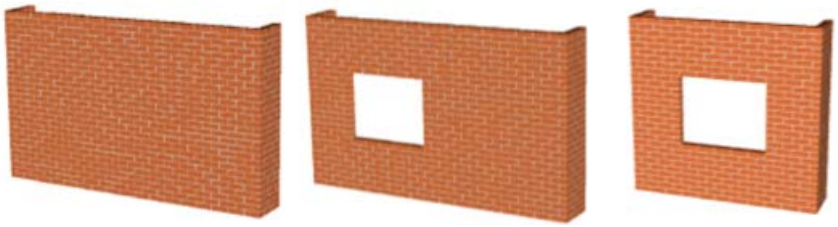

Type A		Type B		Type C	
W1	σ_v = 0.10 MPa	**W3**	σ_v = 0.10 MPa	**W7**	σ_v = 0.10 MPa
W2	σ_v = 0.00 MPa	**W4**	σ_v = 0.05 MPa	**W8**	σ_v = 0.00 MPa
		W5	σ_v = 0.00 MPa		
		W6	σ_v = 0.00 MPa		

4.1 Type A panels (without openings)

A first series of solid panels tested by Griffith and Vaculik (2007) is analysed in the present section. Two rectangular shaped replicates with overall dimensions equal to 4,000 × 2,500 mm^2 were experimentally tested. Two different pre-compression loads (i.e., 0 MPa and 0.10 MPa), as reported in Figure 4, were applied during the laboratory tests. For both walls, simply supported restraints are assumed along the horizontal edges, whereas the two vertical return walls are supposed to be fully clamped through some specific steel profiles. The experimented panels were monitored through a series of displacement transducers located along the walls, whereas the maximum displacement was controlled in correspondence of the centroid of the samples.

The global pressure-displacement curves experimentally obtained are depicted in Figure 5 with the crack patterns obtained at failure for both replicates.

4.2 Type B panels (rectangular shape and eccentric window)

The second series of walls tested belongs to group type B. Such samples are characterised by a rectangular shape with the same global dimensions of type A group, but with an eccentric opening located close to the left hand side. Three different levels of pre-compression (0, 0.05 and 0.1 MPa) were applied respectively in wall W3, W4 and W5. For such replicates, the external restraints as well as the location of the displacement transducers were the same as type A samples.

Panel W6 differs from the others because of the top horizontal edge unsupported. In this latter case, the maximum displacement was monitored through a displacement transducer placed in the middle of the top free edge. The results in terms of pressure-displacement curves for type B replicates are depicted in Figure 6(a), within the crack patterns obtained at failure [Figure 6(b)]. As can be noted, the vertical

pre-compression load, which was varied from 0 MPa for W5 to 0.10 MPa for W3 had the (expected) main beneficial effect of increasing both ductility and peak pressure with a global improvement of the out of plane behaviour. As a matter of fact, the peak pressure ranges from 3.5 MPa to 5 MPa, but the ultimate displacement at failure varied from 13 mm to 20 mm. In this latter case a plateau was experimentally observed (only for panel W3), which is mainly explicable with the higher redistribution of damages along the entire surface of the panel [see for instance the crack pattern of W3 in Figure 6(b)].

Figure 5 (a) Experimental pressure vs. displacement curves (b) Crack patterns obtained at failure for type A masonry walls (see online version for colours)

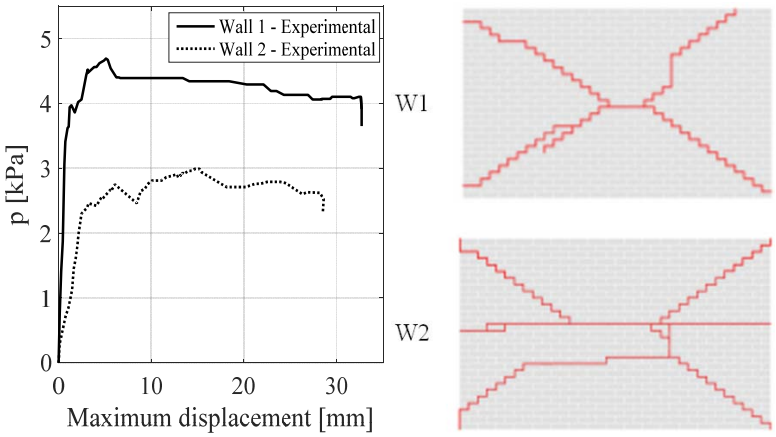

(a) (b)

Figure 6 (a) Experimental pressure vs. displacement curves (b) Crack patterns obtained at failure for type B masonry walls (see online version for colours)

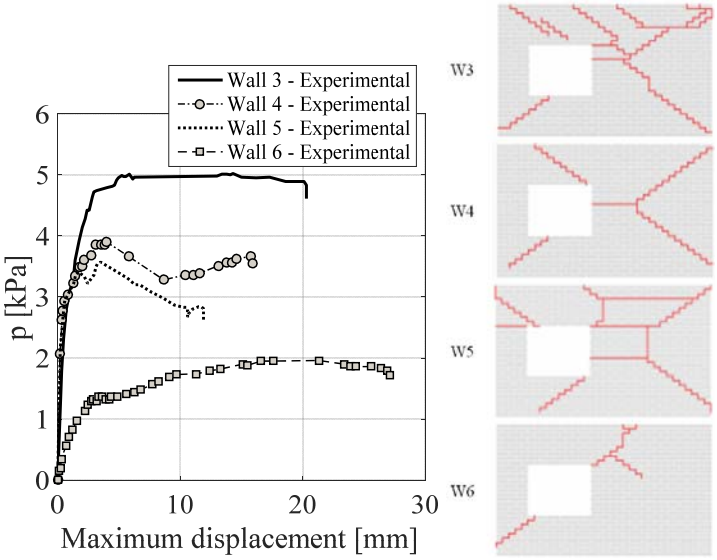

(a) (b)

Panel W6 is characterised by the top edge free to move and rotate. In this case, as expected, both the peak pressure and initial stiffness were lower than the fully supported walls. Even if some diagonal cracks were still present, mainly close to the left hand side corner, the failure of this latter was due to the formation of a vertical central crack that originated in the middle of the wall in correspondence of the unsupported edge. The experimental pressure-displacement curve is shown in Figure 6(a).

4.3 Type C panels (square shape and central window)

The last group of panels tested in the aforementioned experimental campaign is represented by two square walls with a central opening symmetrically placed (see Figure 7). Similarly to the previous groups, the laboratory tests were performed applying a distributed pressure throughout a series of air bags.

Figure 7 (a) Experimental pressure vs. displacement curves (b) Crack patterns obtained at failure for type A masonry walls (see online version for colours)

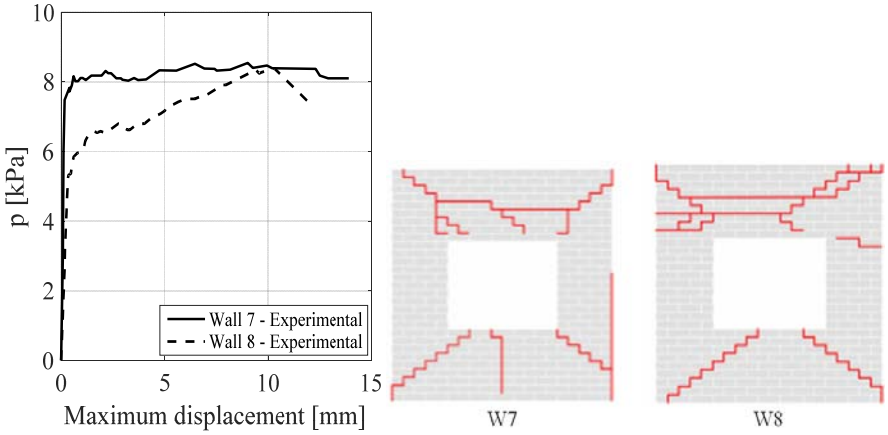

(a) (b)

Similar crack patterns were experimentally observed in both W7 and W8 walls, meaning that the pre-compression load did not influence the collapse mechanism. Indeed, in all cases, on the right side of the panels, severe damages were mainly concentrated along the two diagonals. Stepped cracks developed from the corners of the walls until reaching the central portion of the panel, which failed mainly due to horizontal bending. The presence of the eccentric opening strongly affected the failure mechanism experimentally observed. As a matter of fact, the left side of the walls showed predominant damages close to all corners of the opening, being such zone the weakest.

5 Numerical analyses

In this section, the previously presented series of masonry panels tested by Griffith and Vaculik (2007) is modelled adopting the proposed homogenisation approach. The aim is to verify the accuracy of the two-step homogenisation procedure proposed when dealing with masonry panels subjected to out of plane loads. Accordingly to the experimental

campaign, boundary conditions as well as the level of the pre-compression load are varied. The mechanical properties adopted for bricks and mortar joints are summarised in Table 1, whereas in Table 2 the in plane homogenised elastic properties deduced solving the homogenisation problem at the REV level are reported.

Table 1 Mechanical properties adopted for the constituent materials

Brick	E = 52,700 MPa
	ν = 0.2
Mortar joint	E = 1,000 MPa
	f_t = 0.175 MPa
	f_c = 16 MPa
	c = 1.2 * f_t

Table 2 In plane homogenised mechanical properties: elastic range

Exx	*Eyy*	*Gxy*
19,100 MPa	7,515 MPa	2,510 MPa

The homogenised stress-strain curves obtained and internal stresses on CST elements 1, 2 and 3, assuming a vertical and a horizontal stretching on the REV, are depicted from Figure 8 to Figure 10, respectively. The results, obtained assuming a pure shear deformation state, are shown in Figure 11. The final inelastic homogenised stress-strain curves are depicted in Figure 12–Figure 13 assuming a biaxial strain state and, in Figure 14, imposing a macroscopic shear deformation state to the unit cell. The deformed shapes of the REV at three different steps are also shown from Figure 12 to Figure 14, respectively for each macroscopic deformation state.

Figure 8 Homogenised stress-strain curves obtained for (a) horizontal and (b) vertical stretching of the REV (see online version for colours)

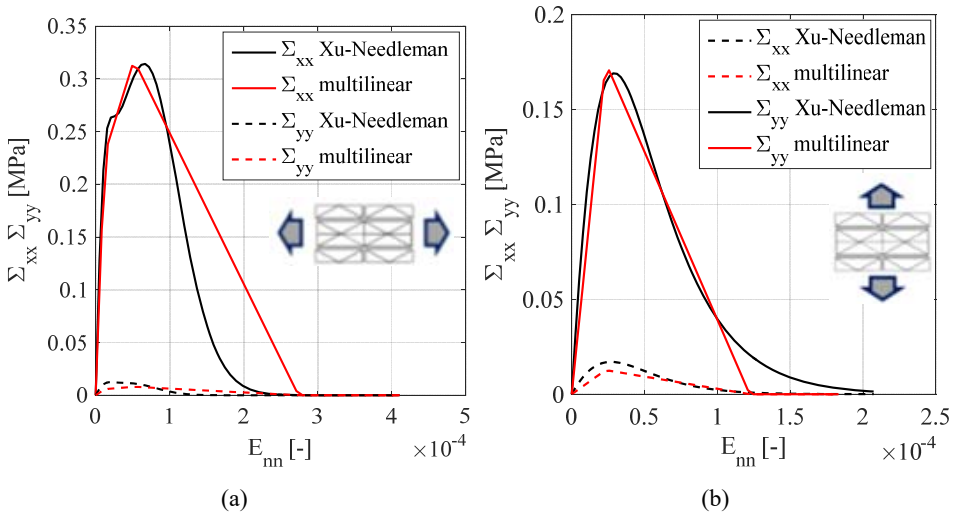

(a) (b)

Figure 9 Horizontal stress-strain curves for CST elements 1, 3 and 2 obtained for (a) horizontal and (b) vertical stretching of the REV (see online version for colours)

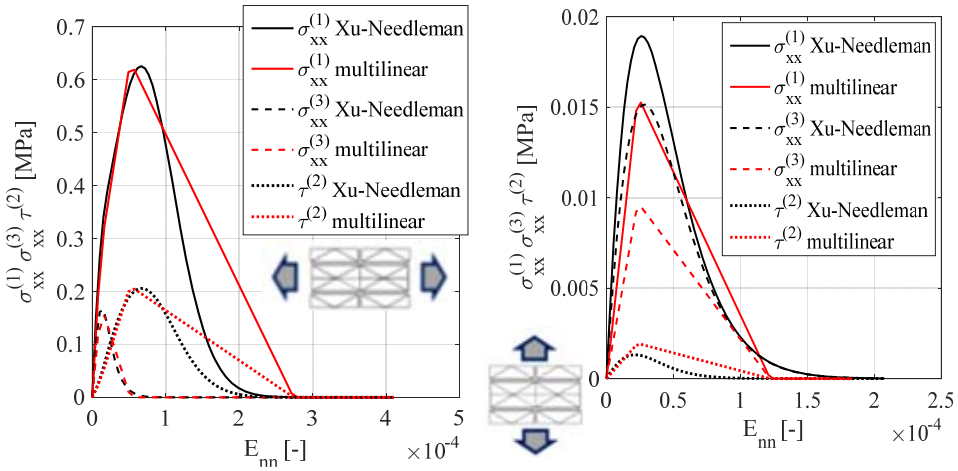

Figure 10 Vertical stress-strain curves for CST elements 1, 3 and 2 obtained for (a) horizontal and (b) vertical stretching of the REV (see online version for colours)

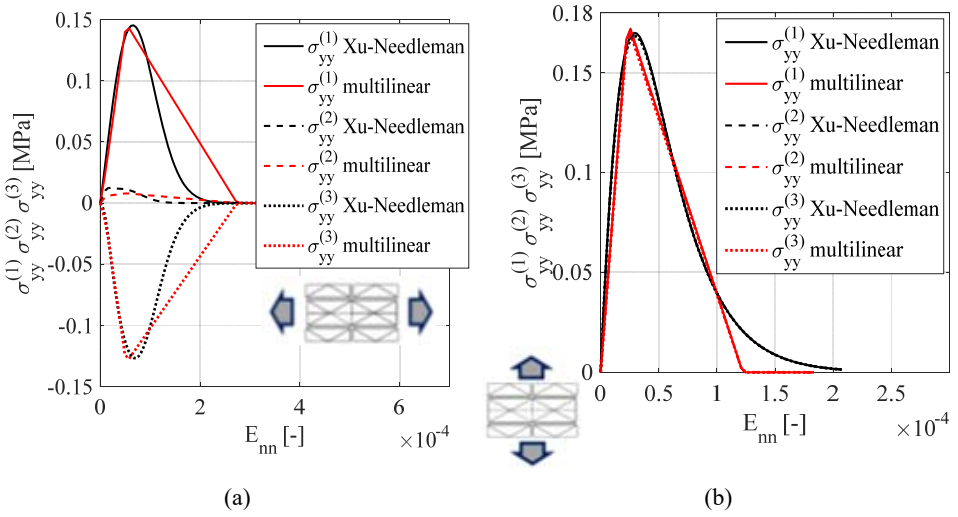

Figure 11 Tangential stress-strain curves obtained applying a pure shear deformation state on the REV, (a) homogenised and (b) on CST 1, 3 elements stresses (see online version for colours)

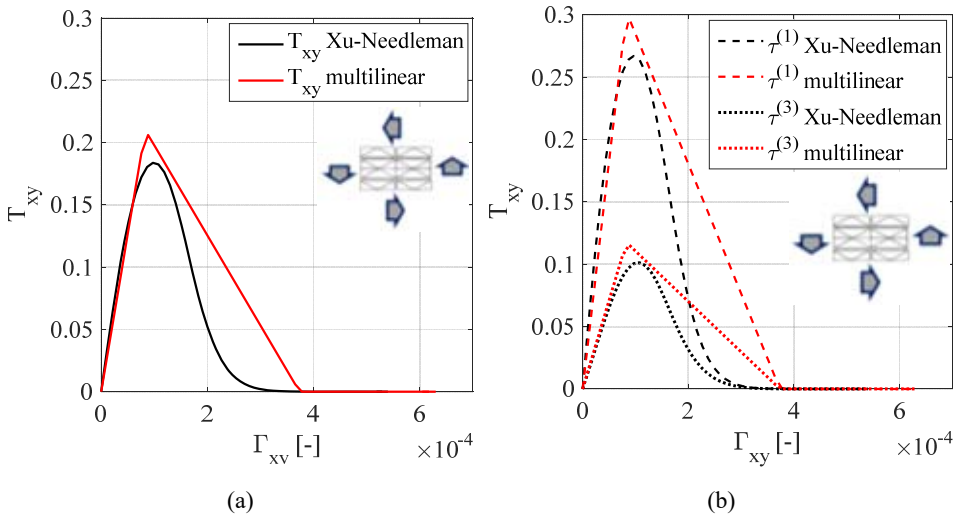

Figure 12 (a) In plane behaviour assuming a horizontal stretching on the REV (b) Deformed shapes at different steps (see online version for colours)

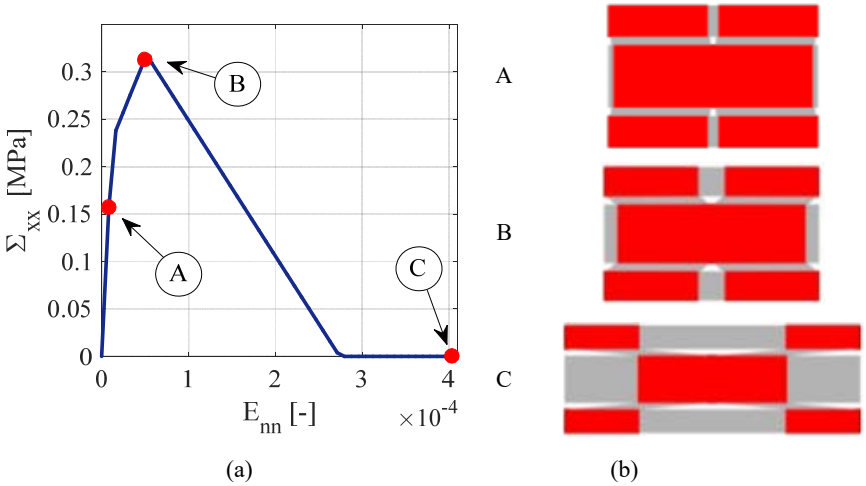

Figure 13 (a) In plane behaviour assuming a vertical stretching on the REV (b) Deformed shapes at different steps (see online version for colours)

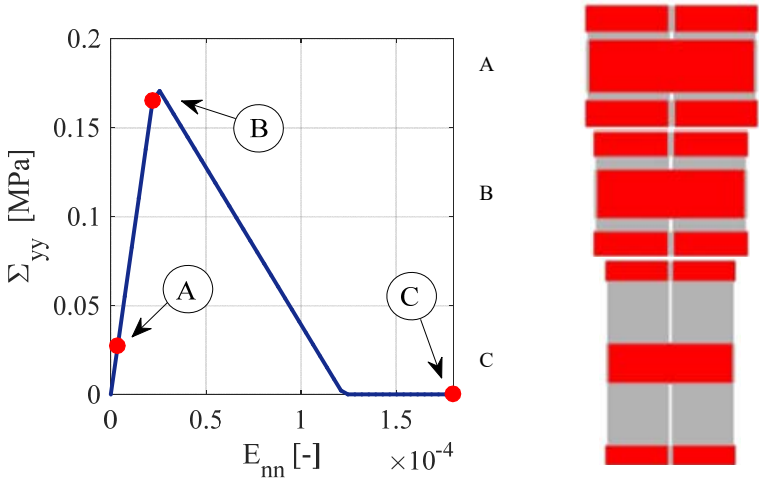

(a) (b)

Figure 14 (a) In plane behaviour assuming a macroscopic shear deformation on the REV (b) Deformed shape at failure (see online version for colours)

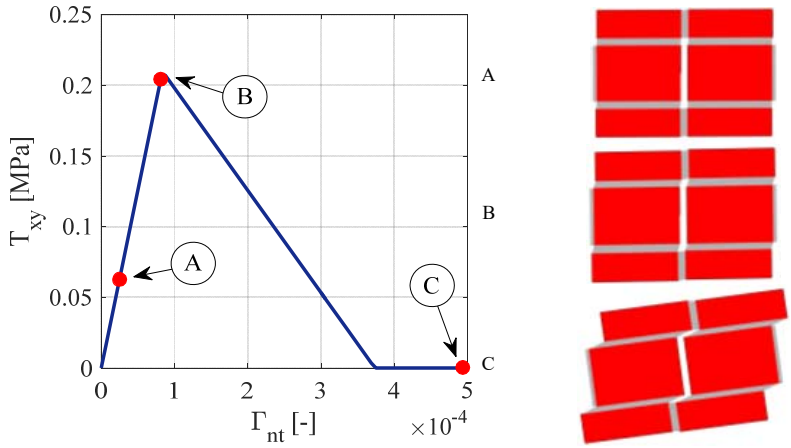

(a) (b)

Figure 15 (a) Out of plane behaviour for vertical bending: moment-curvature curves (b) Stress-strain curves used in the proposed simulations (see online version for colours)

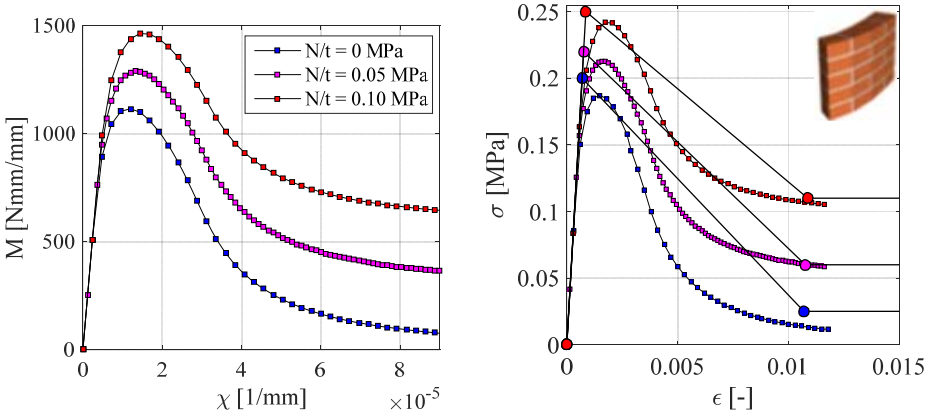

(a) (b)

Starting from the homogenised stress-strain curves obtained at the REV level, the moment-curvature relationships are deduced by on thickness integration. The proposed extension allowed considering both flexural behaviours, such as the vertical and horizontal bending, as well as torsion. To this scope, the RBSM model is slightly modified in order to suitable describe the allowed out of plane behaviours. The identification of the mechanical properties of the out of plane springs has been conducted with an energetic equivalence similar to the in-plane case. The resulting moment-curvature curves are depicted from Figure 15(a) to Figure 17(a), whereas the corresponding stress-strain relationships used at the level of the discrete model are shown from Figure 15(b) to Figure 17(b).

Figure 16 (a) Out of plane behaviour for horizontal bending: moment-curvature curves (b) Stress-strain curves used in the proposed simulations (see online version for colours)

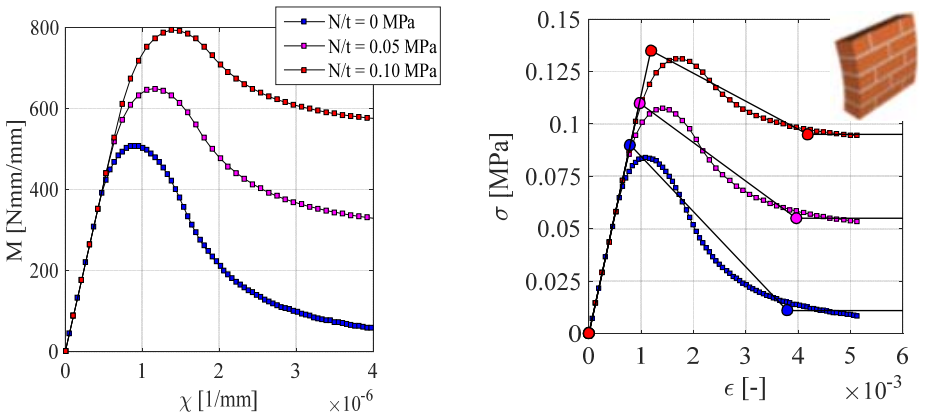

(a) (b)

Figure 17 (a) Out of plane behaviour for torsion: moment-curvature curves (b) Stress-strain curves used in the proposed simulations (see online version for colours)

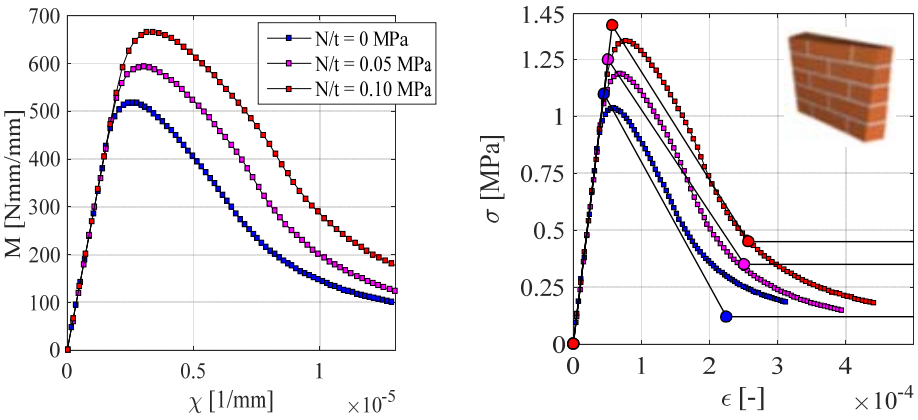

(a) (b)

6 Numerical results

In the present section, the proposed homogenisation approach extended to the out of plane mechanisms is used to simulate three series of masonry panels out of plane loaded. The results obtained, in terms of both global pressure-displacement curves and damage patterns at failure are herein presented and critically discussed. The numerical results are organised into three groups with respect to the types of panels analysed. The proposed distinction is intended to group replicates with the same geometrical features as well as restraint conditions, but with various levels of pre-compression load, to underline the beneficial effect provided by it.

6.1 Type A panels (without openings)

The first group of replicates analysed is represented by type A panels. These walls are indicated in what follows with labels W1 and W2. In this case, no openings are present on the replicates, but two different levels of the pre-compression load are applied during the laboratory tests. An overview of the numerical models and results obtained is provided from Figure 18 to Figure 25. The experimental setup adopted for both panels is shown in Figure 18(a), with the adopted FE discretisation, see Figure 18(b). As can be noted, a coarse mesh is used, namely 851 infinitely resistant quadrilateral elements are used. Out of plane displacements are monitored in a mid-height control point for both the replicates. The restraint conditions and the distributed pressure are applied in the numerical model in agreement with the experimental setup discussed in the previous section. The results are depicted in Figure 18(c) for panel W1 and in Figure 23(c) for panel W2. As can be noted, a satisfactory agreement is found, especially for the first wall.

In this case, both the initial elastic phase as well as the peak pressure are accurately described by the proposed model. In the second wall, severe damages are observed at the very initial stage of the laboratory test, as clearly visible by the sudden change of stiffness of the elastic phase [see Figure 23(c)]. Whilst the numerical model was not able to predict such initial change of stiffness, the peak load found numerically resulted to be very close to the experimental one [see Figure 23(c)]. In both cases, the deformed shapes were very similar. A double curvature response is obtained in both the panels, as depicted, for instance, in Figure 19(d) for the panel W1.

Figure 18 (a) Panel W1 experimental set-up (b) Discretisation adopted for the present simulation, (c and d) Comparison between experimental and numerical results (see online version for colours)

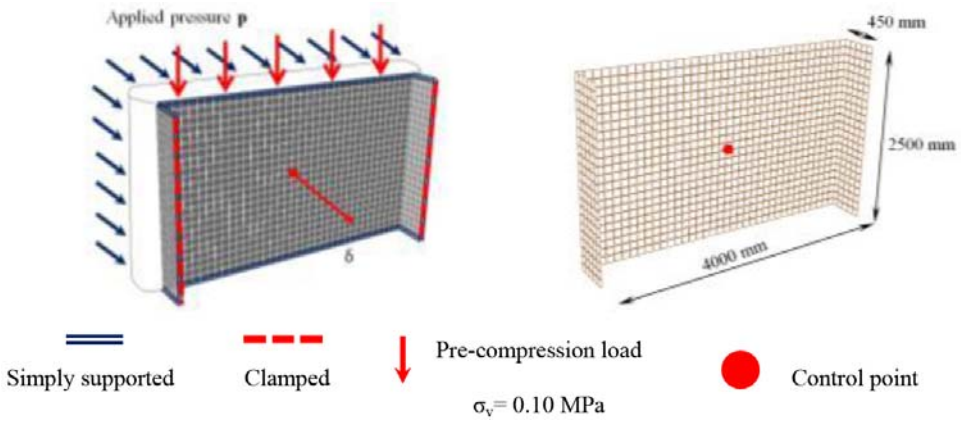

(a) (b)

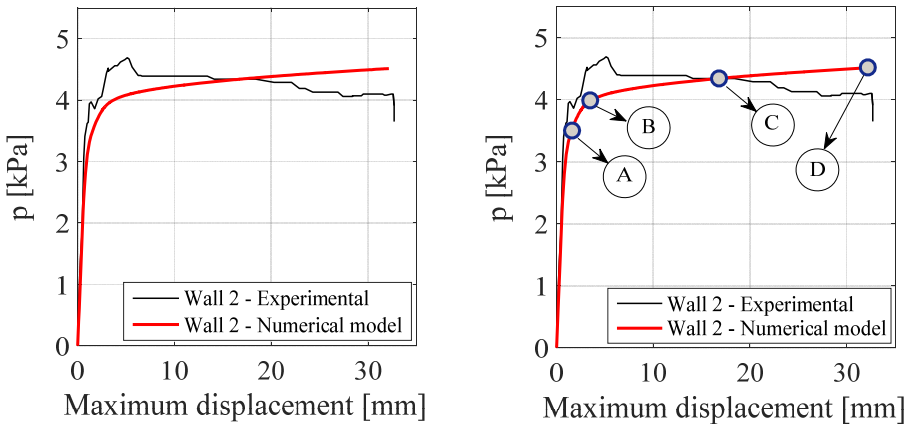

(c) (d)

Figure 19 Panel W1: deformed shapes at different loading steps (magnified 100 times) (see online version for colours)

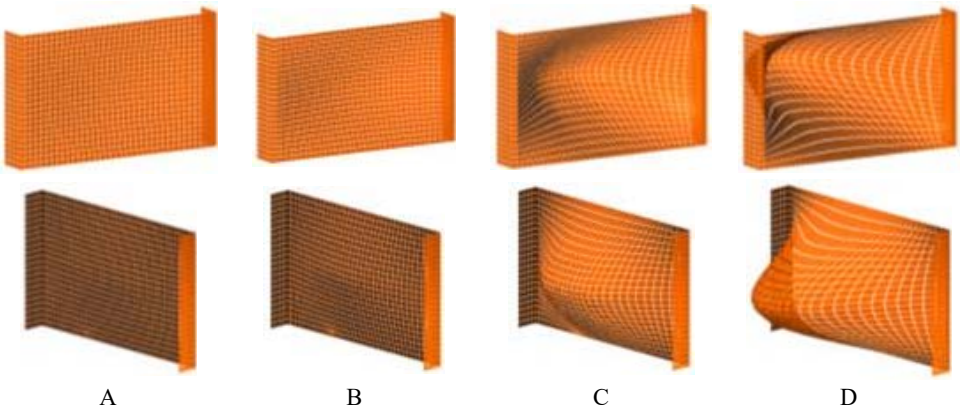

Figure 20 Panel W1 strain patterns at different steps: horizontal bending (magnified 50 times) (see online version for colours)

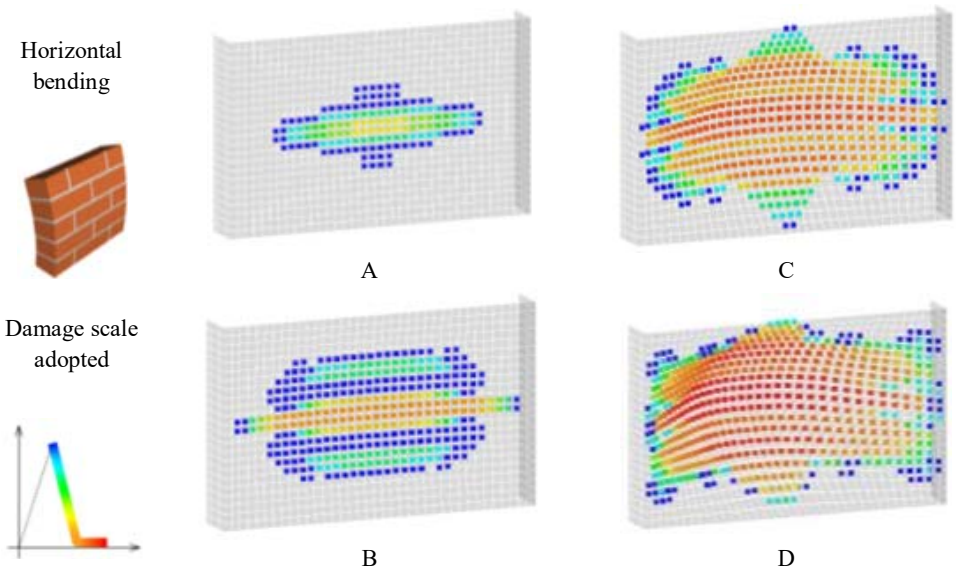

Figure 21 Panel W1 strain patterns at different steps: vertical bending (magnified 50 times) (see online version for colours)

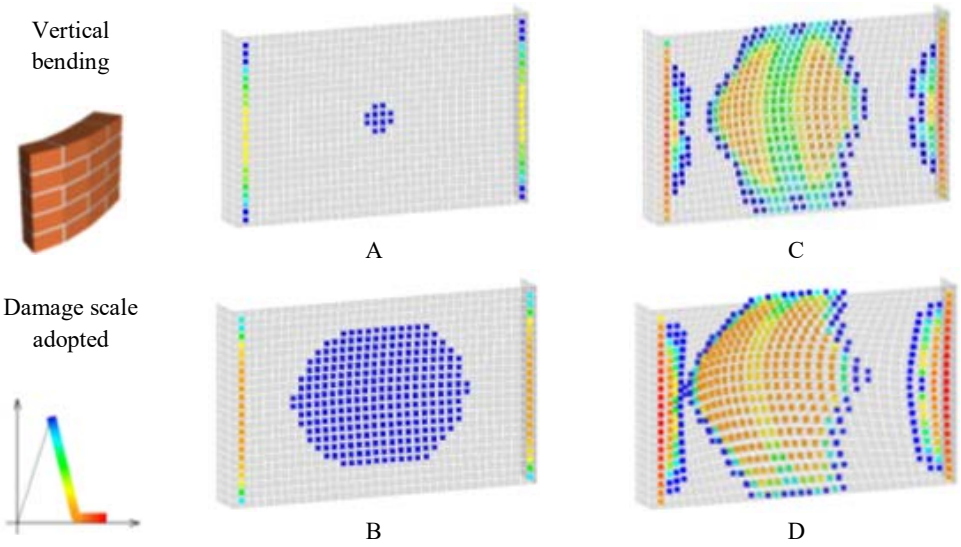

Figure 22 Panel W1 strain patterns at different steps: torsion (magnified 50 times) (see online version for colours)

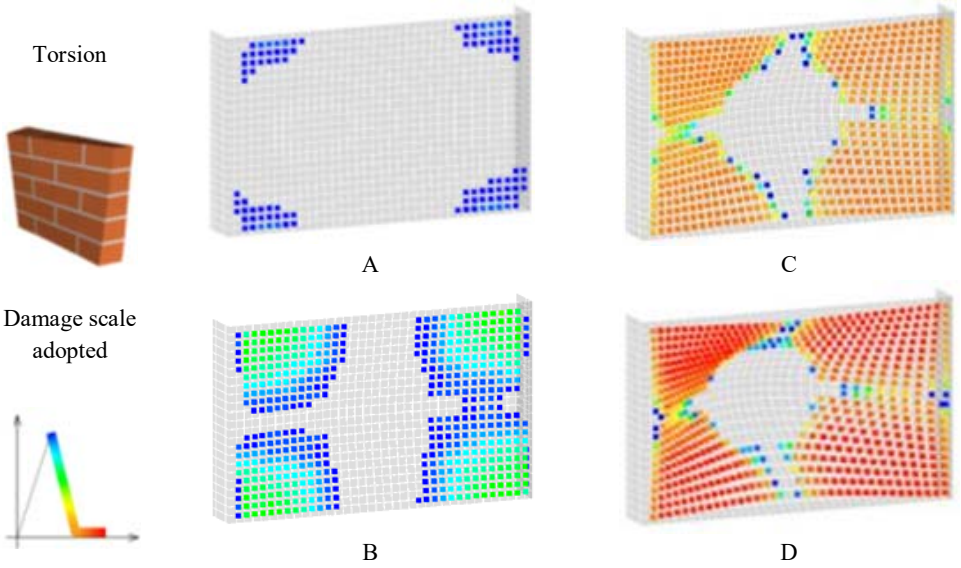

In order to allow a better understanding of the failure mechanism, damage patterns for both the replicates are depicted at different steps during the analyses. Such patterns, referred to panel W1, are provided for horizontal bending (Figure 20), vertical bending (Figure 21) and torsion (Figure 22), separately. It is also important to point out that inelastic strains are plotted instead of damage parameters available into Abaqus (2006). This choice was made essentially because the inelastic strains are related to the damage stored by the deformable elements during the analyses and are immediately available. Indeed, it is possible to couple the maximum level of damage available into the software to the desired inelastic strain independently for compression and tension. Secondly, in this way important information is available about the zones where the inelastic strains are predominant.

Figure 23 (a) Panel W2 experimental set-up (b) Discretisation adopted for the present simulation (c and d) Comparison between experimental and numerical results (see online version for colours)

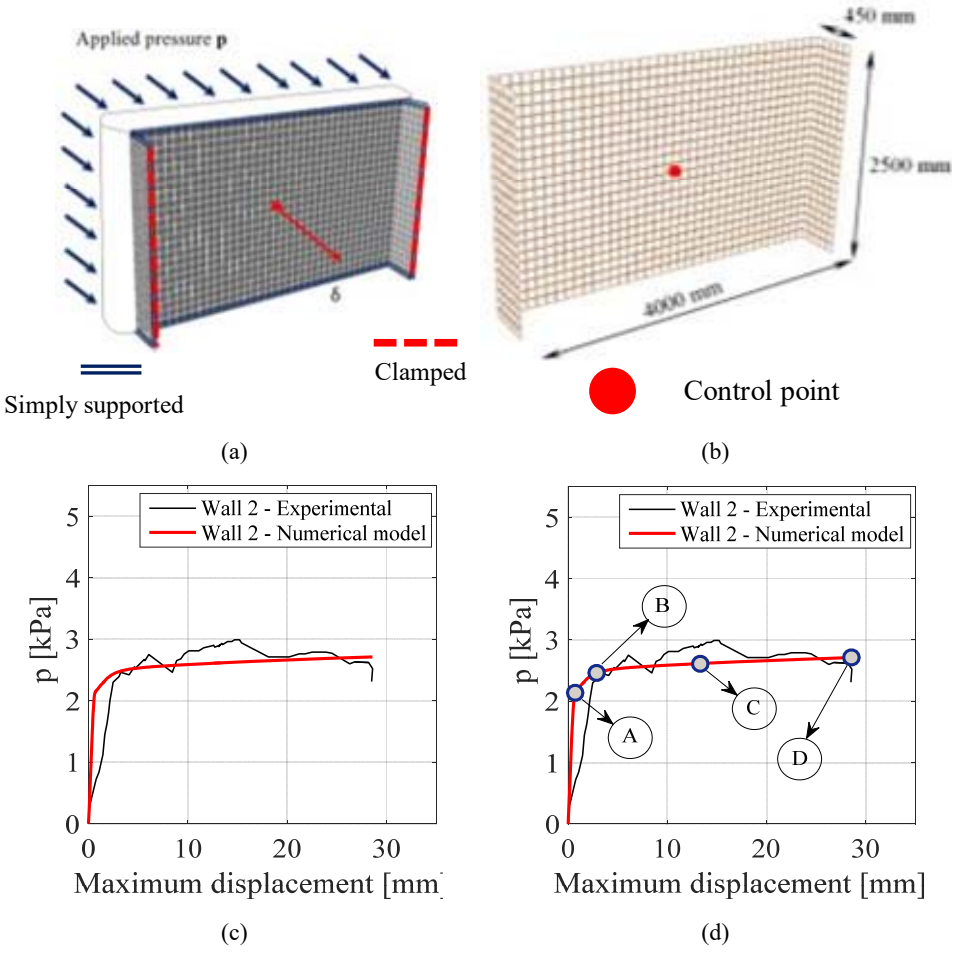

Figure 24 Panel W2 strain patterns at different steps: horizontal bending (magnified 50 times) (see online version for colours)

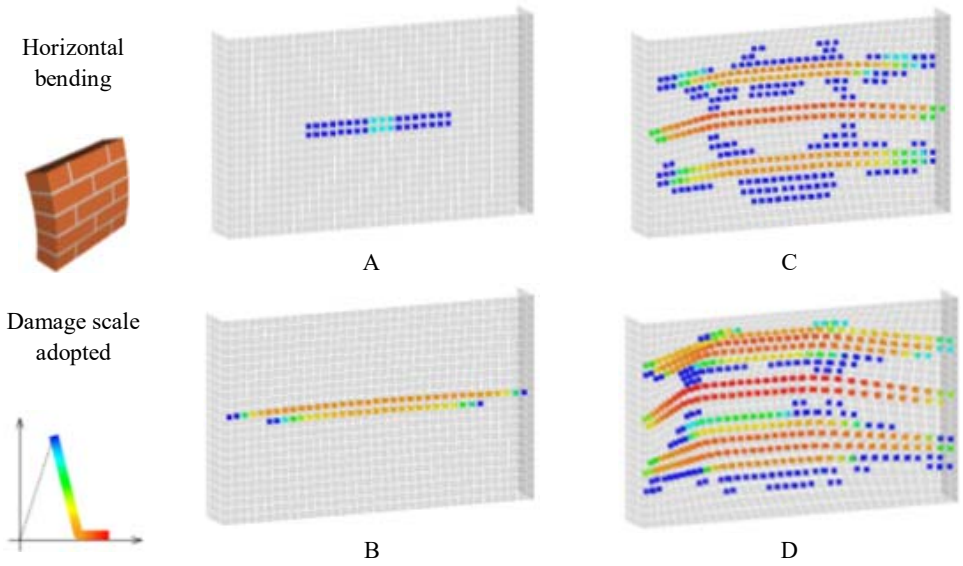

Figure 25 Panel W2: displacement profiles at maximum displacement (see online version for colours)

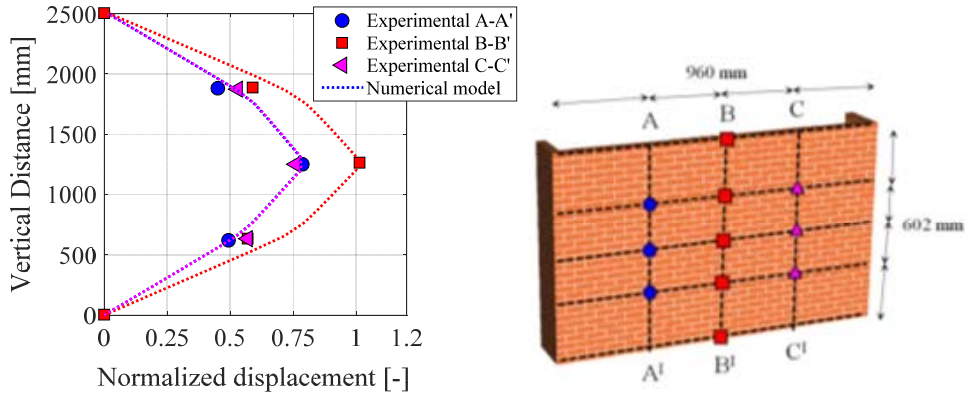

In general, the failure mechanism of panel W2 results to be quite similar to the W1 wall. Central horizontal damages are visible in both panels as well as torsional damages close to the corners. The presence of two return walls allowed providing to the panels a three-dimensional realistic connection similar to what found in existing buildings. As expected, a detachment of the panels from the lateral walls occurred in both replicates. As a matter of fact, panel W1, which is characterised by a pre-compression load of 0.10 MPa, shown a higher level of redistribution of the damages along the entire surface of the wall. Comparing Figure 24(d) with Figure 20(d), it is clearly visible the formation in the first case of three distinct horizontal cracks along the panel, whereas in the second case the damages spread along the entire central portion. Similar findings are obtained for both vertical bending and torsion. Griffith and Vaculik (2007) provided also three

displacement profiles obtained at failure for some panels. The comparison between the experimental results and numerical prediction for panel W2 is depicted in Figure 25, within the position of the displacement transducers used during the laboratory test. As can be noted, a global satisfactory agreement is found. From a numerical point of view, the wall W2 deflected symmetrically up to the failure, such finding is fully in agreement with the experimental evidences.

6.2 Type B (rectangular shape and eccentric window)

A second series of analyses are performed on type B panels. The experimental set-up is shown in Figure 26(a), whereas in Figure 26(b) the mesh adopted during the nonlinear structural analyses is depicted. The panels are discretised with 752 rigid square elements with length edge equal to 100 mm. According to the experimental set-up, the external action of the airbags is reproduced with a pressure uniformly distributed along the outer surface of the walls. The verse of the positive deflections is indicated in Figure 26(a) within the position of the control point. It is worth noting that the position of the displacement transducer as well as the distributed pressure applied during the simulations are maintained for the first three panels. The external restraints are similar to the previous set of simulations.

The numerical results are here compared to the corresponding experimental evidences. Only one parameter is varied for the first three panels, whereas the fourth is discussed later.

The numerical results are compared with the experimental ones in Figures 26(c), 26(d) and 26(e), respectively for walls W3, W4 and W5. In all cases, a satisfactory agreement in terms of initial elastic stiffness and peak load is found. The collapse mechanism is studied plotting the inelastic strain developed during the analyses along the entire panel at failure for bending and torsion interfaces separately. As confirmed by the experimental evidences, the presence of the eccentric opening strongly influences the collapse mechanism. High values of inelastic deformations originated close to the corners of the opening and propagated towards the wall corners (see Figure 27). The failure of the panels is however due to the horizontal flexion of the central portion of the walls that undergoes severe inelastic deformations, as confirmed by the tensile damage patterns depicted in Figure 27. The progressive damaging mechanism is however similar in all the replicates of this group. Considering panel W5 as reference, the collapse mechanism is clearly visible: the damages originate in the middle horizontal interfaces of the panel and spread towards the lower and upper right-hand side corners, indicating a combination of horizontal flexural failure, mainly concentrated in the central part of the panel, and torsional failure close to the wall corners (see Figure 27). A partial detachment of the front panel with respect to the lateral walls is also observed in all the replicates.

Figure 26 (a) Experimental set-up (b) Discretisation adopted for the present simulations, comparison between experimental and numerical results for (c) W3 (d) W4 (e) W5 panels (see online version for colours)

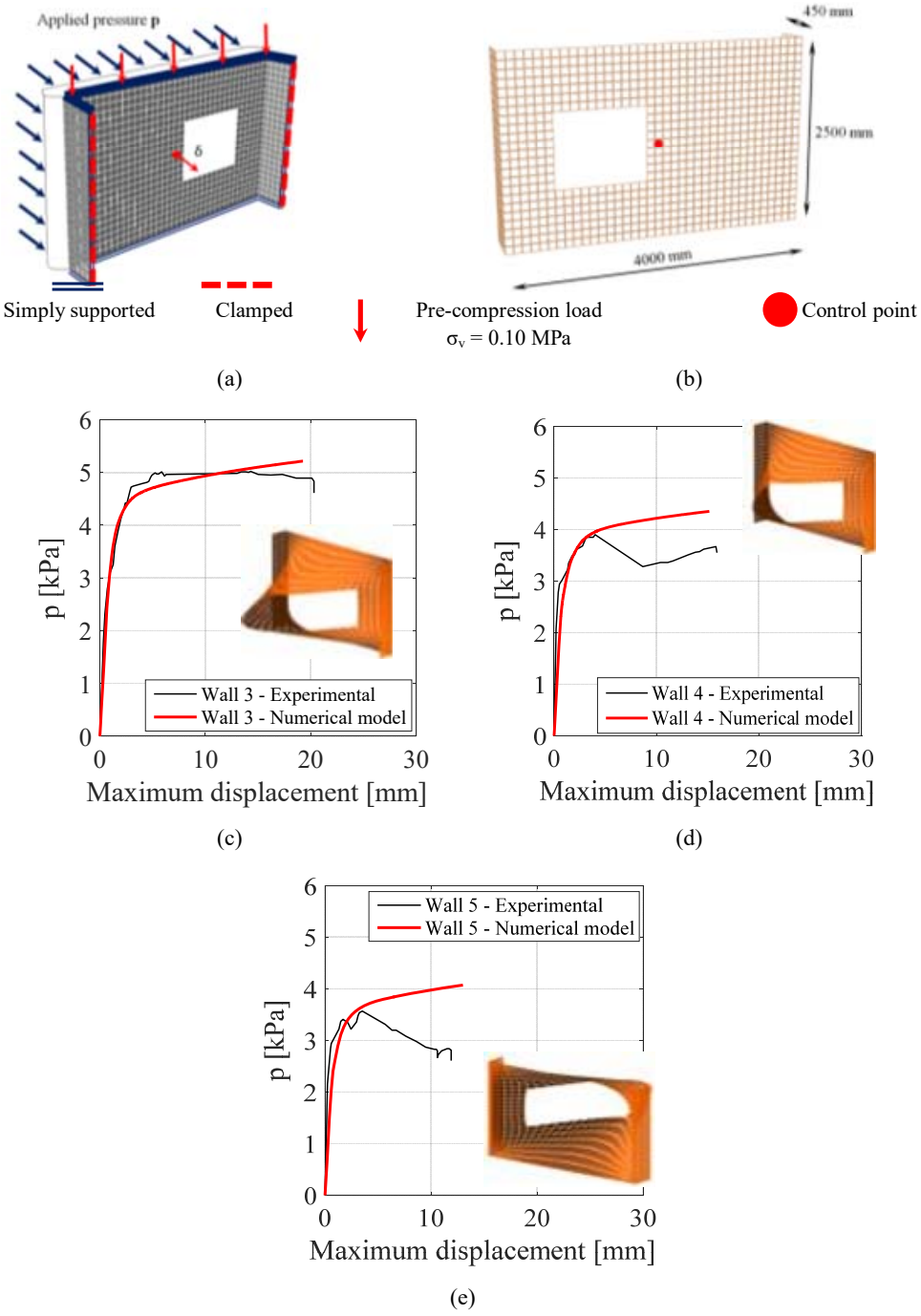

Figure 27 Damage patterns at failure obtained for W3-W4 and W5 panels (magnified 100 times) (see online version for colours)

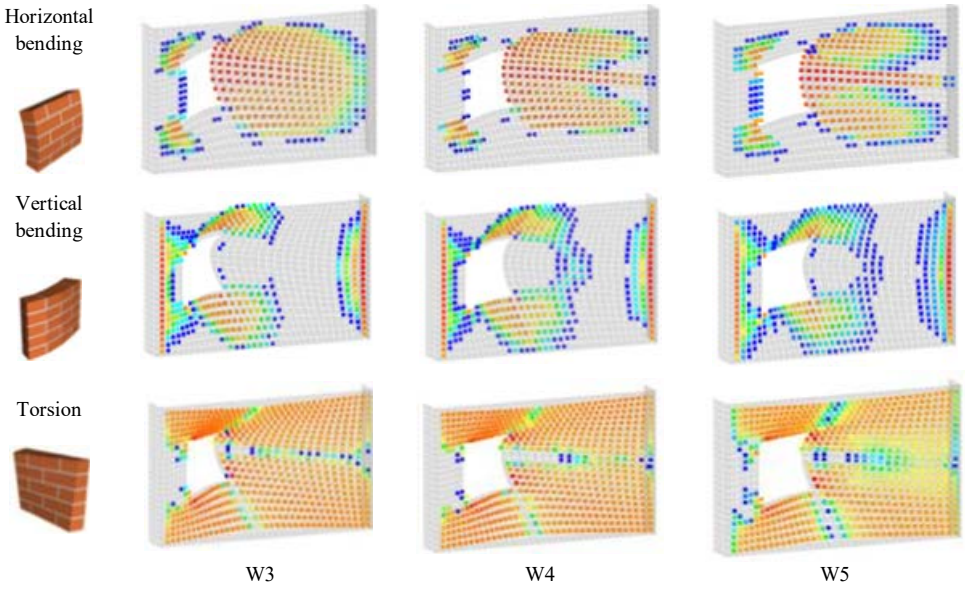

The deformed shape of wall W5 was experimentally monitored using a series of displacement transducers placed on the surface of the panel. The resultant experimental displacements near failure are reported in Figure 28 and compared with the numerical outcomes. As expected, a generally good agreement is found. Larger differences are obtained in the lateral regions of the wall.

Figure 28 Panel W5: experimental and numerical normalised displacement profiles near failure (see online version for colours)

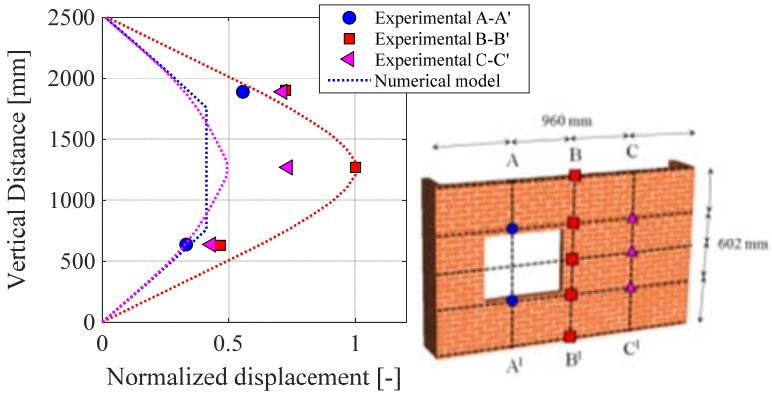

The last type of walls analysed in the present group is represented by panel W6. In this case, the simple support of the horizontal top edge was removed and left free. The experimental set-up of the wall is depicted in Figure 29(a), within the position of the control point and the external restraint assumed during the simulations. As can be noted, the discretisation adopted in the previous models is maintained. A comparison between

the numerical predictions and the experimental results is depicted in Figure 29(b). As expected, a satisfactory agreement is found even in this case in terms of peak load. Limited differences are observed in the initial phase, being the proposed model stiffer than the experimental one.

Figure 29 (a) Panel W6 experimental set-up (b) Comparison between experimental and numerical results (see online version for colours)

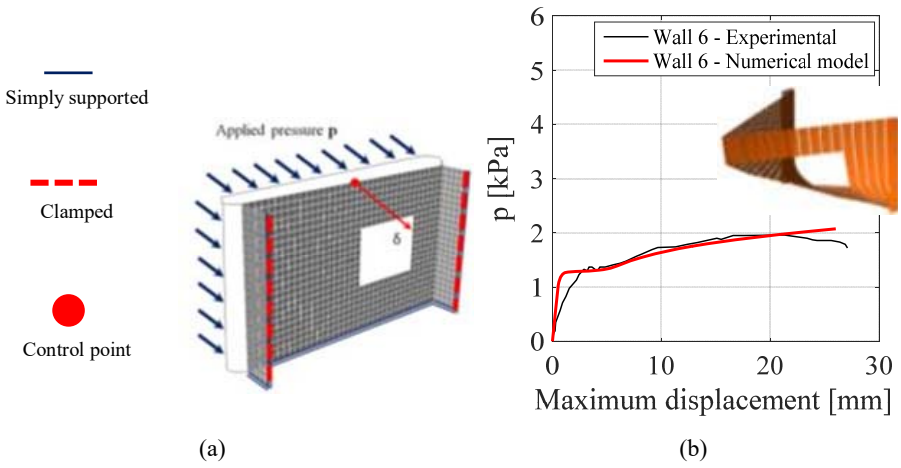

Even in this case, the failure mechanism is studied plotting the inelastic strains for the three types of interfaces employed during the simulations. The corresponding damage patterns are depicted in Figure 30, respectively for horizontal bending, vertical bending and torsion. As clearly visible, the inelastic strains are localised mainly along a vertical central crack [see Figure 30(b)] as well as close to the corners of the wall [see Figure 30(b)].

Figure 30 Panel W6 strain patterns at failure, (a) horizontal (b) vertical bending (c) torsion (see online version for colours)

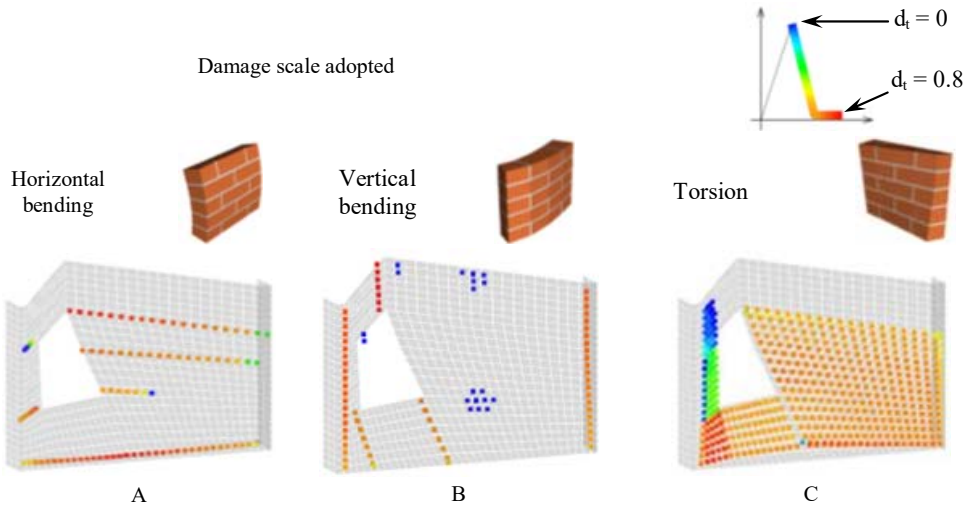

Figure 31 Panel W6: displacement profiles at maximum displacement (see online version for colours)

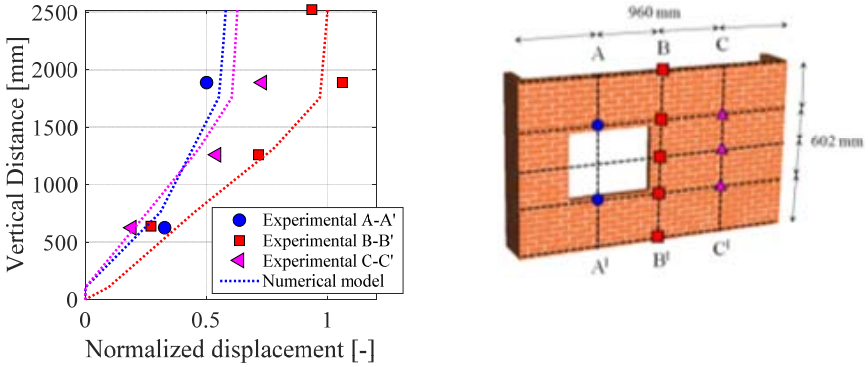

Even in this case, the displacement profiles experimentally found are available for comparison purposes. A comparison between the experimental results and the numerical outcomes is depicted in Figure 31. A satisfactory agreement is found. The model is able to accurately describe not only the global behaviour of such panel, but also the deformed shape at maximum displacement.

Figure 32 (a) Panel W7 experimental set-up (b) Discretisation adopted for the present simulation (c and d) Comparison between experimental and numerical results (see online version for colours)

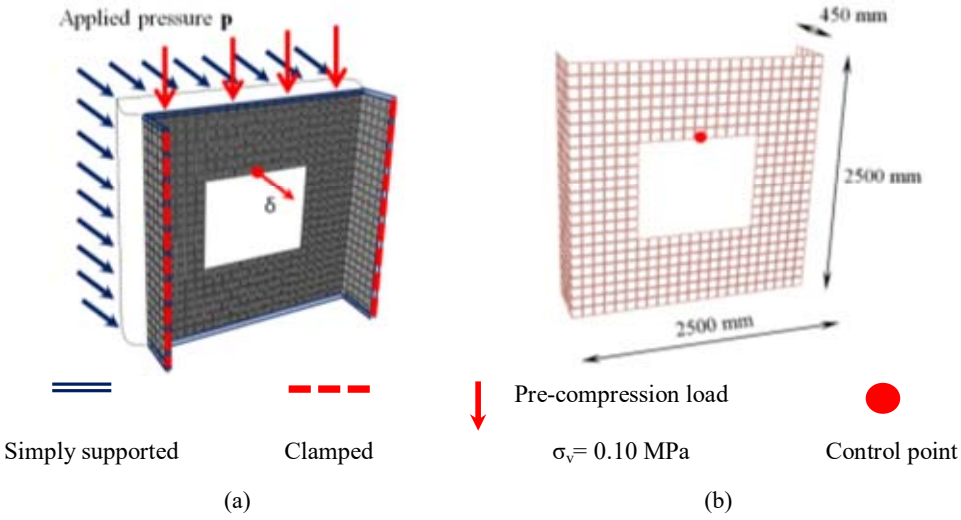

Figure 32 (a) Panel W7 experimental set-up (b) Discretisation adopted for the present simulation (c and d) Comparison between experimental and numerical results (continued) (see online version for colours)

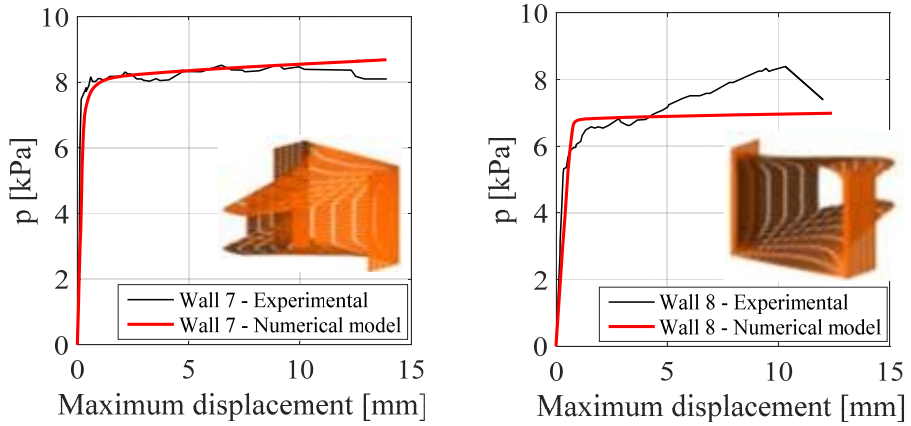

Figure 33 Damage patterns at failure obtained with the numerical model for W7 and W8 panels (magnified 100 times) (see online version for colours)

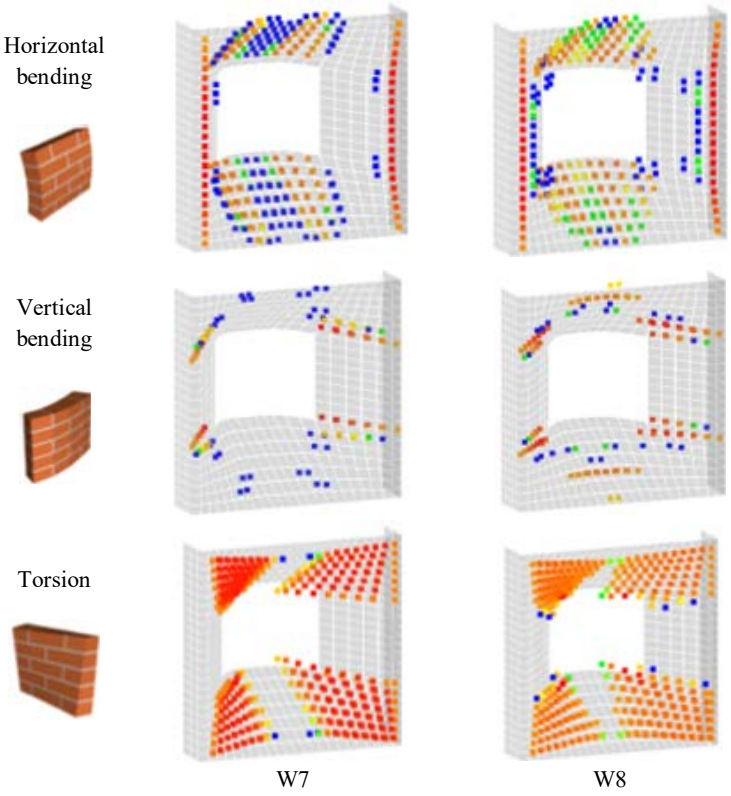

6.3 Type C (square shape and central window)

The last group of panels is indicated with the label type C. Two square replicates are analysed using the proposed homogenisation approach. In agreement with the experimental set-up, a uniformly distributed pressure was applied on the outer surface of the walls [see Figure 32(a)], whereas the external restraints were maintained unchanged with respect to the other cases. The discretisation adopted for both the simulations is depicted in Figure 32(b) with the position of the control point. The results found experimentally and those obtained with the proposed approach are compared in Figure 32(c) and 32(d), respectively for wall W7 and W8. A satisfactory agreement is found for the first wall, whereas slight differences are observed for the second one. A good correspondence is found in the description of the first elastic phase and the peak pressure for both panels. In both cases, the failure mechanism is mainly influenced by the detachment of the front panel from the lateral walls (see Figure 33). In addition, damages spread in correspondence of the corners towards the opening along the principal diagonals (see Figure 33).

7 Conclusions

The present paper is intended to assess the accuracy of a proposed homogenisation approach extended to out of plane loaded masonry. To this scope, a RBSM model, previously formulated to describe in plane loaded masonry structures is slightly modified to allow flexural and torsional deformations. The model is benchmarked against a series of full scale unreinforced masonry panels tested by Griffith and Vaculik (2007). The proposed experimental investigation considered several aspects, in order to match closely the conditions of existing buildings. Among the others, the most important aspects are the presence of eccentric or symmetrically located openings, the level of pre-compression loads and the 2D external restraints.

All these aspects were properly taken into account in the proposed simulations. In particular the walls were subdivided into three groups in order to better understand the influence of specific parameters on the global behaviour of such panels. All the proposed simulations were performed using the commercial FE software Abaqus. The elastic with softening behaviour of the deformable interfaces was modelled using the concrete damage plasticity model available in Abaqus. A general satisfactory agreement was found comparing the numerical predictions and the experimental results, for all the panels analysed. Furthermore, the failure mechanisms were properly described plotting the inelastic strains at different steps up to failure and subdividing damages among horizontal, vertical bending and torsion. Only for some walls tested, displacement profiles near failure were available, the numerical model proving in such cases a good fitting with experimental data. In conclusion the adopted homogenisation procedure resulted particularly suitable for an accurate description of the failure mechanisms active, fitting quite well also the global pressure-displacement curves obtained during the laboratory tests.

At last, it is important to address the possibility of extending the use of the model to study random masonry, multi-leaf walls, reinforced masonry or other masonry patterns. Likewise, it can be applied to study larger structures in the context of a professional or academic purpose.

References

Abaqus (2006) *Finite Element Analysis (Theory Manual)*, Providence: RI, Dassault Systèmes Simulia Corporation.

Augenti, N. and Parisi, F. (2010) 'Learning from construction failures due to the 2009 L'Aquila, Italy, earthquake', *Journal of Performance of Constructed Facilities*, Vol. 24, No. 6, pp.536–555.

Baraldi, D. and Cecchi, A. (2017) 'A full 3D rigid block model for the collapse behaviour of masonry walls', *European Journal of Mechanics – A/Solids*, Vol. 64, pp.11–28 [online] http://www.sciencedirect.com/science/article/pii/S0997753817300669 (accessed 22 May 2018).

Bertolesi, E., Milani, G. and Lourenço, P.B. (2016) 'Implementation and validation of a total displacement non-linear homogenization approach for in-plane loaded masonry', *Computers & Structures*, Vol. 176, pp.13–33 [online] http://www.sciencedirect.com/science/article/pii/S0045794916307428 (accessed 22 May 2018).

Borri, A. (2004) 'Analisi ed interventi su edifici esistenti in muratura (in Italian)', in *XI Convegno ANIDIS, l'ingegneria sismica in Italia*, Genova.

Brandonisio, G. et al. (2013) 'Damage and performance evaluation of masonry churches in the 2009 L'Aquila earthquake', *Engineering Failure Analysis*, Vol. 34, pp.693–714 [online] http://www.sciencedirect.com/science/article/pii/S1350630713000319 (accessed 22 May 2018).

Capurso, M. (1971) 'Limit analysis: two-dimensional structures (in Italian)', in *Tamburini Editore for Italsider S.p.a.*, Genova.

Casolo, S. (1999) 'Rigid element model for non-linear analysis of masonry façades subjected to out-of-plane loading', *Communications in Numerical Methods in Engineering*, Vol. 15, No. 7, pp.457–468.

Cecchi, A., Milani, G. and Tralli, A. (2005) 'Validation of analytical multiparameter homogenization models for out-of-plane loaded masonry walls by means of the finite element method', *Journal of Engineering Mechanics*, Vol. 131, No. 2, pp.185–198 [online] http://ascelibrary.org/doi/abs/10.1061/(ASCE)0733-9399(2005)131:2(185) (accessed 22 May 2018).

Çelebi, M. et al. (2010) 'Recorded motions of the 6 April 2009 Mw 6.3 L'Aquila, Italy, earthquake and implications for building structural damage: overview', *Earthquake Spectra*, Vol. 26, No. 3, pp.651–684 [online] https://doi.org/10.1193/1.3450317 (accessed 22 May 2018).

Craig, G.M. et al. (2004) 'Experimental investigation of unreinforced brick masonry walls in flexure', *Journal of Structural Engineering*, Vol. 130, No. 3, pp.423–432 [online] https://doi.org/10.1061/(ASCE)0733-9445(2004)130:3(423) (accessed 22 May 2018).

Dazio, A. (2008) 'The effect of the boundary conditions on the out-of-plane behaviour of unreinforced masonry walls', in *Proceedings of the 14th World Conference on Earthquake Engineering*, Innovation, Practice, Safety, Chinese Association of Earthquake Engineering, 12–17 October 2008, Beijing, China.

de Buhan, P. and de Felice, G. (1997) 'A homogenisation approach to the ultimate strength of brick masonry', *Journal of the Mechanics and Physics of Solids*, Vol. 45, No. 7, pp.1085–1104.

de Felice, G. and Giannini, R. (2001) 'Out-of-plane seismic resistance of masonry walls', *Journal of Earthquake Engineering*, Vol. 5, No. 2, pp.253–271 [online] https://doi.org/10.1080/13632460109350394 (accessed 22 May 2018).

Griffith, M. and Magenes, G. (2003) 'Evaluation of out-of-plane stability of unreinforced masonry walls subjected to seismic excitation', *Journal of Earthquake Engineering*, Vol. 7, No. 141, pp.141–169.

Griffith, M.C. and Vaculik, J. (2007) 'Out-of-plane flexural strength of unreinforced clay brick masonry walls', *TMS Journal*, Vol. 25, No. 1, pp.53–68.

Guggisberg, R. and Thürlimann, B. (1990) 'Failure criterion for laterally loaded masonry walls', in *Proc., 5th North Am. Masonry Conf.*, pp.949–958.

Johnson, D. (1996) 'Automated yield-line analysis of orthotropic slabs', *International Journal of Solids and Structures*, Vol. 33, No. 1, pp.1–10 [online] http://www.sciencedirect.com/science/article/pii/0020768395000256 (accessed 22 May 2018).

Lemos, J.V. (2007) 'Discrete element modeling of masonry structures', *International Journal of Architectural Heritage*, Vol. 1, No. 2, pp.190–213.

Milani, G. and Bertolesi, E. (2017) 'Quasi-analytical homogenization approach for the non-linear analysis of in-plane loaded masonry panels', *Construction and Building Materials*, Vol. 146, No. 15, pp.723–743 [online] http://doi.org/10.1016/j.conbuildmat.2017.04.008.

Milani, G., Lourenço, P.B. and Tralli, A. (2005) 'A micro-mechanical model for the homogenized limit analysis of out-of-plane loaded masonry walls', in *Civil-Comp 2005: 10th Inter. Conf. on Civil, Structural and Environmental Engineering Computing*, Rome, Italy.

Milani, G., Lourenço, P.B. and Tralli, A. (2006) 'Homogenised limit analysis of masonry walls, part I: failure surfaces', *Computers & Structures*, Vol. 84, No. 3, pp.166–180 [online] http://www.sciencedirect.com/science/article/pii/S0045794905003159 (accessed 22 May 2018).

Mojsilovic, N. and Marti, P. (1994) *Tests on Masonry Walls Subjected to Combined Actions*, Institute of Structural Engineering, ETH Zurich, Switzerland.

Orduña, A. (2003) *Seismic Assessment of Ancient Masonry Structures by Rigid Blocks Limit Analysis*, University of Minho, Guimarães, Portugal.

Parisi, F. and Augenti, N. (2013) 'Earthquake damages to cultural heritage constructions and simplified assessment of artworks', *Engineering Failure Analysis*, December, Vol. 34, pp.735–760.

Reccia, E. et al. (2014) 'Full 3D homogenization approach to investigate the behavior of masonry arch bridges: the Venice trans-lagoon railway bridge', *Construction and Building Materials*, Vol. 66, pp.567–586 [online] http://www.sciencedirect.com/science/article/pii/S0950061814005984 (accessed 22 May 2018).

Sab, K. (2003) 'Yield design of thin periodic plates by a homogenization technique and an application to masonry walls', *Comptes Rendus Mécanique*, Vol. 331, No. 9, pp.641–646 [online] http://www.sciencedirect.com/science/article/pii/S163107210300144X (accessed 22 May 2018).

Shawa, O.A. et al. (2012) 'Out-of-plane seismic behaviour of rocking masonry walls', *Earthquake Engineering & Structural Dynamics*, Vol. 41, No. 5, pp.949–968.

Sincraian, G. (2001) *Seismic Behaviour of Blocky Masonry Structures. A Discrete Element Method Approach*, IST, Lisbon, Portugal.

Sinha, B.P. (1978) 'A simplified ultimate load analysis of laterally-loaded model orthotropic brickwork panels of low tensile strength', *Structural Engineering ASCE*, Vol. 56B, No. 4, pp.81–84.

Sinha, B.P. (1980) 'An ultimate load analysis of laterally loaded brickwork panels', *International Journal of Masonry Construction*, Vol. 1, No. 2, pp.57–61.

Sutcliffe, D.J., Yu, H.S. and Page, A.W. (2001) 'Lower bound limit analysis of unreinforced masonry shear walls', *Computers & Structures*, Vol. 79, No. 14, pp.1295–1312 [online] http://www.sciencedirect.com/science/article/pii/S0045794901000244 (accessed 22 May 2018).

Wilhelm, M., Mojsilovic, N. and Dazio, A. (2007) 'Out-of-plane shaking table tests on unreinforced masonry walls', in *Proceedings of the 10th North American Masonry Conference*, St. Louis, MO, USA.